Interface structure of Fe/Ag multilayers prepared by pulsed laser deposition

Ratnesh Gupta,[1,*] Martin Weisheit,[2] Hans-Ulrich Krebs,[2] and Peter Schaaf[1,†]
[1]*Zweites Physikalisches Institut, Universität Göttingen, Bunsenstrasse 7-9, 37073 Göttingen, Germany*
[2]*Institut für Materialphysik, Universität Göttingen, Hospitalstrasse 5, 37073 Göttingen, Germany*
(Received 24 July 2002; published 5 February 2003)

Fe/Ag multilayers with single layer thicknesses in the nanometer range have been deposited on Si(100) using pulsed laser deposition. Conversion electron Mössbauer spectroscopy in conjunction with Rutherford backscattering spectrometry and x-ray reflectivity have been used for the evaluation of the interface structure of these multilayers. In the Fe-Ag system, with a large positive heat of mixing, a solid solution of bcc Fe(Ag) has been found by placing an enriched ^{57}Fe marker layer at different distances to the multilayer interfaces. The interface structure mainly depends on dynamic effects during the deposition processes. From the analyses, we have obtained an asymmetric intermixing at lower and upper interfaces of the individual Fe layers: the intermixing of Fe into Ag is lower than that of Ag into Fe. The studies of the interface structure were performed by varying parameters such as the thickness of the elemental layers and the target-to-substrate distance during the deposition process.

DOI: 10.1103/PhysRevB.67.075402 PACS number(s): 68.65.Ac, 76.80.+y, 34.50.Dy, 82.65.+r

I. INTRODUCTION

Pulsed laser deposition (PLD) is a well-established technique for the deposition of thin films and multilayers.[1,2] It involves the formation of a laser-induced plasma and the subsequent deposition of the plasma species on a substrate. Plasma temperatures as high as 10^5-10^7 K have been reached by this method.[1,2] The characteristics of the PLD technique for the formation of thin films have been found to differ significantly from other deposition methods. The instantaneous growth rate during PLD is substantially higher than the growth rate during sputter deposition.[3] High flux and high energies of the particles reaching the substrate seem to be particularly propitious for the growth of metastable phases. The quenching rate is of the same order of magnitude as those of sputtered particles. This method has especially attractive features: it allows easy preservation of stoichiometry and good structural quality of the deposited films, even when grown at rather low temperatures.

For a better understanding of the growth mechanisms, the nature and transport of species from the target to the substrate have to be known and controlled. Contrary to conventional desorption and evaporation, in laser ablation, particles generally undergo a large number of collisions and thus make the final distribution very different from nascent ones. Moreover, the atomic species in a conventional thermal process primarily consist of neutral atoms and molecules but the laser-generated plasma is composed of neutral and ionized atoms, molecules, and other species.[4,5] Granular Fe/Ag thin films showed an effect of giant magneto-resistance and this effect mainly depends on several preparation parameters.[6] In the present paper, we investigated the interface structure of Fe/Ag multilayers by varying the geometry of the specimens and other process parameters such as the target-to-substrate distance.

In equilibrium, Fe and Ag are completely immiscible, and the heat of mixing between Fe and Ag is strongly positive ($\Delta H_{mix}=+42$ kJ/mol) at equiatomic composition. Even in the liquid state ($\Delta H_{mix}=+28$ kJ/mol),[7] there is no tendency towards intermixing. However, the PLD process may be expected to be similar to that of ion-beam mixing[8] or vapor quenching.[9]

Mössbauer spectroscopy in conjunction with other complementary analytical techniques has been used to get closer information on the interface structures. The ^{57}Fe isotope has been used to find the interface structure at different positions in a single Fe layer, enabling us to obtain some knowledge about the transport of the species during the deposition process.

II. EXPERIMENT

For the preparation of Fe/Ag multilayers, 30 ns laser pulses from a KrF excimer laser ($\lambda=248$ nm) with an energy density of 6–7 J/cm^2 at a repetition rate of 9 Hz were used. The multiple-target/multiple-substrate setup is described elsewhere.[10–12] Along with natural Fe, a 95%-enriched ^{57}Fe probe layer was used at some specific places in the multilayers. Four different sets of specimens were prepared. The thickness of the individual layers of Ag (t_{Ag}) and Fe (t_{Fe}) was the same in all the sets of specimens

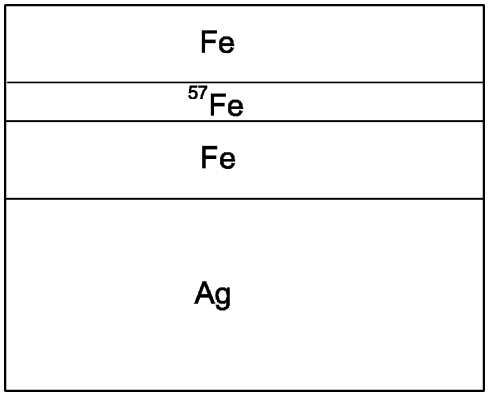

FIG. 1. Schematic specimen geometry for specimen B3, set C, and set D.

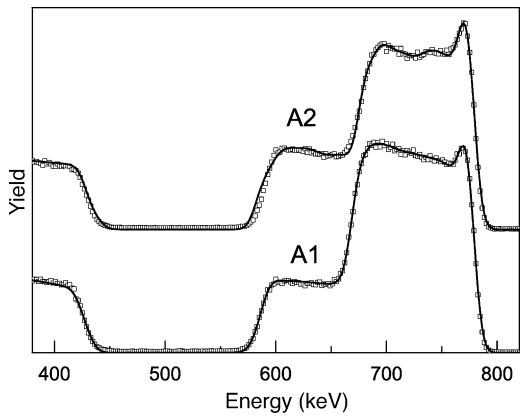

FIG. 2. Fitted RBS spectra of the Fe/Ag multilayers A1 and A2 with the periodicities $\Lambda = 2.3$ nm ($N = 40$) and 3.8 nm ($N = 20$).

($t_{Ag} = t_{Fe}$). In set A, the geometry of the specimen was [Si(100)/[Ag/^{57}Fe]× N/Ag] with two different periodicities ($\Lambda = t_{Ag} + t_{Fe}$). In one case, it was $\Lambda = 3.8$ nm and in the other $\Lambda = 2.3$ nm while N stands for the number of bilayers ($N = 20$ and 40, respectively).

The geometry of specimen set B was {Si(100)/[Ag/Fe(1)/Fe(2)/Fe(3)/Fe(4)/Fe(5)] × 20/Ag}. The periodicity of the specimens was 5.0 nm, where $[\Lambda = t_{Ag} + t_{Fe(1)} + t_{Fe(2)} + t_{Fe(3)} + t_{Fe(4)} + t_{Fe(5)}]$, keeping the total thickness of Fe equal to that of the Ag layer. In this set B, we prepared five different specimens by placing a ^{57}Fe probe layer (thickness 0.5 nm) at different positions, namely, in the case of specimen B1, Fe(1) was replaced by enriched ^{57}Fe while the other four layers of Fe were natural. In the case of specimens B2, B3, B4, and B5, ^{57}Fe was deposited in the positions of Fe(2), Fe(3), Fe(4), and Fe(5), respectively.

In set C, we prepared specimens equivalent to specimen B3 and varied the target-to-substrate distance from 50 mm to 100 mm ($\Lambda = 5.0$ nm). A schematic diagram of the specimen geometry is given in Fig. 1. In the cases of sets A and B, the target-to-substrate was always 80 mm.

In set D, we followed the geometry of specimen B3 and the target-to-substrate distance was 68 mm. The geometry of the specimens was {Si(100)/[Ag/Fe(1)/Fe(2)/^{57}Fe(3)/Fe(4)/Fe(5)] × N /Ag}. The number N was either 10, 5, or 2 while Λ was 10, 20, or 50 nm for the specimens D1, D2, and D3, respectively.

The films were deposited at room temperature onto Si(100) substrates placed parallel to the target at the given distance. The deposition chamber also contained an Auger electron spectrometer (AES), so that the produced surface films could be analyzed *in situ* by the AES. After deposition, the samples were analyzed by means of Rutherford backscattering spectrometry (RBS), using the 900-keV He^{++} beam of the Göttingen 530-kV accelerator IONAS.[13] The energy spectrum of the backscattered He^{++} ions was measured using a silicon barrier detector at a backscattering angle of 165° with respect to the normal incidence beam. The detector resolution was about 13 keV and the typical values for the beam current were between 5 and 15 nA. The program WINDF was used for the analysis of the RBS spectra.[14]

TABLE I. Average concentration of Fe and Ag in the multilayers and total thicknesses estimated by the depth profiles of Fe and Ag as obtained by fitting the RBS spectra. The values given in parentheses represent the standard deviation.

Sample	Thickness (nm)	Fe (%)	Ag (%)
A1	79(5)	47(2)	53(2)
A2	67(5)	53(2)	47(3)
B1	123(5)	39(4)	62(3)
B2	126(5)	38(4)	62(3)
B3	126(5)	35(4)	65(2)
B4	126(5)	38(3)	62(2)
B5	118(5)	36(3)	64(2)
D1	80(5)	57(2)	43(2)
D2	82(5)	50(2)	50(2)
D3	94(5)	52(2)	48(2)

Conversion electron Mössbauer spectra (CEMS) were measured in a constant acceleration mode with a 15-mCi ^{57}Co/Rh source and a gas flow (94% He, 6% CH_4) proportional counter.[15] The spectra were analyzed by superimposing Lorentzian lines with a least-squares-fit program.[16]

III. RESULTS AND DISCUSSION

Figure 2 shows the RBS spectra of the Fe/Ag multilayer specimens A1 and A2 with the periodicities of $\Lambda = 3.8$ nm ($N = 20$ periods) and $\Lambda = 2.3$ nm ($N = 40$ periods). Both spectra look similar with sharp peaks at the Ag edge, resulting from the top layer consisting of Ag. Other layers are not resolved due to their small thicknesses. From the fitting of the RBS spectra, one can estimate the total thicknesses of the samples and the overall stoichiometry. The corresponding depth profiles give the average atomic concentration of the two species. The resulting values are given in Table I.

The Mössbauer spectra of the two specimens A1 and A2 are presented in Fig. 3. The spectrum of sample A1 consists of a broad sextet structure. The spectra were analyzed assuming three sextets (M0, M1, M2) and one doublet (d). The doublet d represents Fe atoms located in an fcc Ag matrix, in

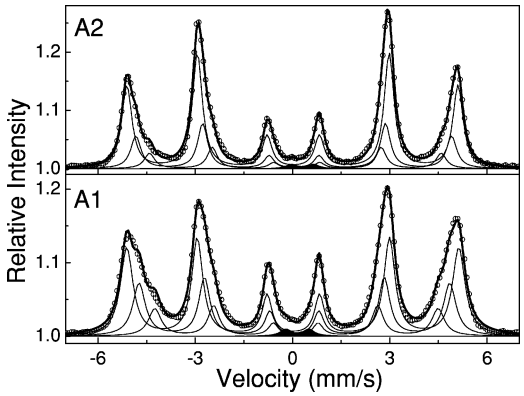

FIG. 3. Fitted CEMS of Fe/Ag multilayers A1 ($\Lambda = 2.3$ nm) and A2 ($\Lambda = 3.8$ nm). Experimental data points are shown by hollow spheres and the fitted subspectra are indicated by solid lines.

TABLE II. Relative abundance (area fraction in %) of the different subspectra as evaluated by CEMS analysis. The values given in parentheses represent the standard deviation.

Sample	M0	M1	M2	d
A1	68(2)	21(2)	8(2)	3(2)
A2	44(2)	28(2)	26(2)	2(2)
B1	56(2)	29(2)	13(2)	2(2)
B2	75(2)	16(2)	7(2)	2(2)
B3	48(2)	31(2)	18(2)	3(2)
B4	38(2)	35(2)	25(2)	2(2)
B5	31(3)	39(2)	28(2)	2(2)
D1	87(2)	10(2)		3(2)
D2	95(3)	3(2)		2(2)
D3	92(2)	5(2)		3(2)

accordance with previous measurements.[8,10,17–19] The magnetic subspectra M0–M2 correspond to the bcc-Fe phase, where some Ag atoms are substitutionally incorporated, giving rise to some Fe atoms having one, two, or more Ag atoms in their nearest neighborhood. The hyperfine fields are linearly decreasing with the number of Ag nearest neighbors (nn).[17,18] The mean values found here are 32.0(1) T (M0), 30.5(3) T (M1), and 28.3(5) T (M2).[20,21] Thus, M0 corresponds to Fe atoms having no direct Ag neighbors, M1 to those having one, and M2 to those having two or more Ag neighbors. The magnetic hyperfine field B_{hf} of Fe nuclei is dependent on the actual environment of the nuclei. B_{hf} decreases with the number of neighboring nonmagnetic Ag atoms. It is mostly affected by the nearest neighbors. Nevertheless, more distant Ag neighbors also affect the hyperfine field. Therefore, the hyperfine field is also influenced by the layer thickness and the overall Ag concentration.[17,18] Doublet d shows no magnetic interaction, therefore it originates from Fe nuclei in a nonmagnetic environment. The doublet is broad, indicating structural disorder, and it suggests that one, two, or more Fe atoms and defects segregate in the fcc-Ag lattice.

The spectral areas of the different components for both the specimens are given in Table II. The relative abundance of the sextets M1 and M2 slightly increases for the multilayer with the smaller periodicity. This means that there is more Ag in the bcc phase, i.e., there is more intermixing between the individual layers in the thinner multilayer structure, as one would also expect. Moreover, the relative line intensity ratios change with periodicity. For $\Lambda = 3.8$ nm all subspectra show the magnetization orientation in the layer plane, because the line intensity ratio of the second (I2) and fifth (I5) lines with respect to the inner third (I3) and fourth lines was I2/I3=4.0(2). For $\Lambda = 2.3$ nm the intensity ratio was I2/I3=2.0(3), which suggests that the spins are more randomly oriented.

The RBS spectra of the specimens B1–B5 are shown in Fig. 4. The spectra look identical for all samples, thus the multilayer structures of these films are identical, as they should be (^{57}Fe and ^{56}Fe are just distinguishable with RBS at this energy for the ideal case, but here the difference is very small); the total thickness and average concentration of

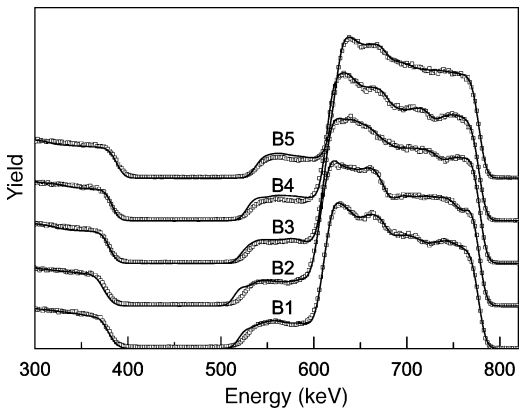

FIG. 4. Fitted RBS spectra of Fe/Ag multilayers with a periodicity of 5.0 nm of sample set B (specimens B1–B5).

Fe and Ag have been obtained by fitting the RBS spectra, the values are depicted in Table I, and they agree within the error limits. Figure 5 shows the CEMS spectra of samples B1–B5. The ^{57}Fe marker layer, which is only sensitive to Mössbauer spectroscopy, was introduced at various positions within the idividual natural iron sublayers. The position of the marker layer was changed in identical steps of 0.5 nm from the lower interface (B1) to the upper interface (B5) with a periodicity of 5.0 nm (20 periods), thus giving information on the processes between the Ag/Fe interfaces and the Fe/Ag interfaces. Thus, the information collected has different origins and information about the processes that occurred dur-

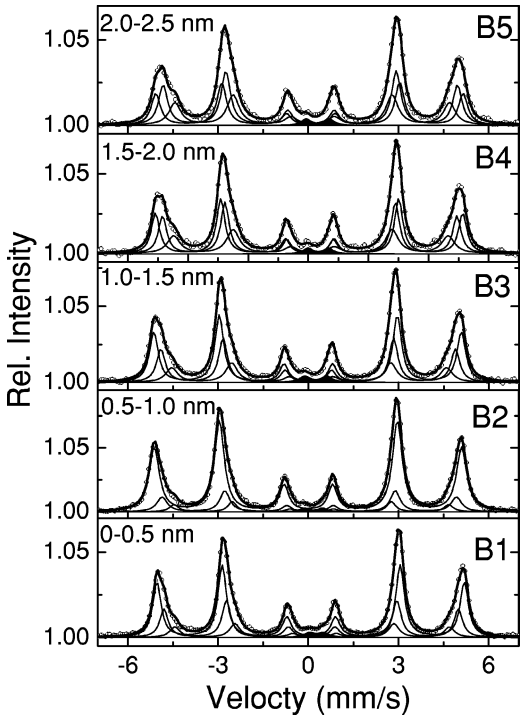

FIG. 5. Fitted CEMS of Fe/Ag multilayers with $\Lambda = 5.0$ nm for specimens B1–B5. The distance of the ^{57}Fe marker layer from the lower Ag/Fe interface is given. Experimental data points are shown by hollow spheres, and fitted subsprectra are indicated by solid lines.

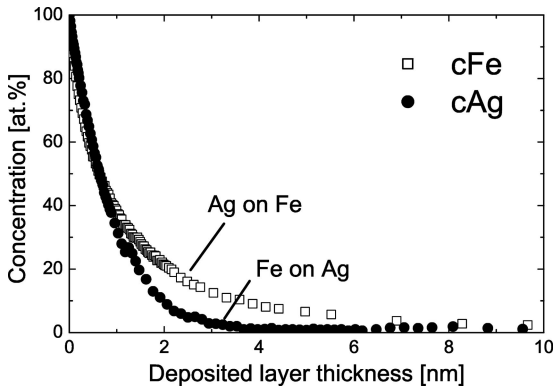

FIG. 6. Ag concentration profile for Fe deposited on top of Ag (●) and Fe concentration for Ag deposited on top of Fe (□) obtained from *in situ* Auger electron spectroscopy (AES).

ing deposition inside the layers may be extracted. From low angle x-ray reflectivity, one can also estimate the exact periodicity on the basis of the first-order Bragg peaks. The estimated thicknesses of B1, B3, and B5 are 5.1(0.3), 5.4(0.3), and 5.6(0.3) nm, respectively.

The Mössbauer spectra were fitted by the same procedure as mentioned above. All four components (M0, M1, M2, and doublet d) are present in all the spectra with a slight variation of the hyperfine parameters within the error limits. The hyperfine fields of the sextets were first fitted freely and then adjusted to their mean values in order to achieve a better accuracy in the relative abundances of the subspectra, which sensitively depend on the hyperfine fields. The mean values are 31.7 T (M0), 30.4 T (M1) and 28.4 T (M2). Table II gives the relative spectral areas of the Mössbauer components M0, M1, M2, and d. There are no changes in the relative line intensities of the sextet within the error limits for these samples. Table II reveals that the abundance of M1 and M2 in sample B5 is quite high compared to B1. Here, one may note that in the case of B1 the marker layer ^{57}Fe is deposited on Ag while in the case of B5, Ag is deposited on the ^{57}Fe marker. A similar behavior can also be observed for B2 and B4. Thus we can say that the concentration of Ag atoms located inside the iron layer (iron lattice) is higher for depositing Ag onto Fe than vice versa. From Table II, one may also observe that the relative spectral area of α-Fe (M0) decreases steadily from sample B2 to B5. We have obtained similar results in *in situ* Auger electron spectroscopy during the deposition process, as shown in Fig. 6, where the Fe concentration was measured during deposition of Ag onto Fe and the Ag concentration was measured during deposition of Fe onto Ag. Fe covers Ag much faster than Ag covers Fe, indicating a larger intermixing when depositing Ag.

The relative variation of the concentrations in the case of Ag/Fe (sample B1) and Fe/Ag (sample B5), besides the asymmetric intermixing, may be due to the dissolution mode which depends strongly on the temperature and the difference in surface energy between the deposit and the substrate. For systems with a phase-separation tendency such as Fe-Ag, before the inevitable total dissolution, the deposited atoms will try to form clusters or layers in order to minimize the number of heteroatomic neighbors. These clusters or layers can either remain at the surface or be embedded in the substrate layer depending on the sign of the difference in surface energy. Such studies have been performed in Fe/Cu, where the heat of mixing is positive as well.[22,23] However, one may note that due to the lattice mismatch the interfacial disorder is larger while depositing Ag on Fe than that of Fe on Ag. In equilibrium, Ag only occurs in the fcc structure, whereas Fe can exist both in fcc and bcc phases (for thin films). During the process of PLD, the energy of the deposited ions and atoms was measured to be in the range of 10–200 eV.[10] According to the theory of energy loss in matter, the range of Ag deposited onto Fe and vice versa can be estimated to be 1 nm for Ag onto Fe and 2 nm for Fe onto Ag (at 100 eV), i.e., Fe originally penetrates deeper into Ag than Ag into Fe.[24,25] Ma *et al.*[26] have also observed that high-energy ball milling of Fe and Ag powders does not produce any solid solutions, not even at liquid-nitrogen temperature. In contrast to this, they could prepare a solid solution of Fe-Cu at room temperature under similar conditions. Both systems are immiscible and exhibit a positive heat of mixing (the difference is that Fe/Cu is miscible in the liquid phase). They argue that the mixing of Fe and Ag exists on the atomic level along with the demixing process between the two elements, and, therefore, the mixing and demixing processes simultaneously occur. Consequently, it is not possible to make any substantial changes in the powders. Recent experiments on small angle x-ray scattering of Fe-Cu, prepared by ball milling, suggest large heterogeneities on a nanometer scale.[27,28] Similar behavior can also be predicted in the present case: the mobility of Fe in Ag is higher than that of Ag in Fe. The same holds for the reverse process, hence the concentration of energetic Fe atoms in Ag atoms is lower than that of Ag atoms in Fe atoms, as we have observed in samples B1 and B2. Due to the dissipated kinetic energy of the impinging species, their internal excitation energies, and their heat of condensation and desorption, the temperature on the substrate surface changes during and between laser pulses. The rise in temperature enhances the de-mixing process in the system. In an x-ray study of ion-beam mixing of Fe/Ag multilayers, Krebs *et al.* proposed that ballistic mixing in the collisional phases of the recoil cascade is counterbalanced by demixing and phase separation in the thermal spike phase.[11]

Figure 7 gives the CEMS of the specimens deposited by varying the target-substrate distance. ^{57}Fe is placed in the middle of the individual iron layers and its thickness is nominally 0.5 nm. The spectra look quite similar. The total thicknesses of the specimens were determined by fitting the corresponding RBS profile, shown in Fig. 8. The average concentration of Fe and Ag is 50(3)%, each. In this case, instead of three magnetic sextets, we used four magnetic sextets assuming one more sextet (M3) with a field of 27.5 T and a larger number of Ag neighbors (three and more) in iron than for the magnetic sextet M2.

We plotted the spectral areas of the different magnetic sextets and doublets in Fig. 9. This figure suggests that with increasing target-substrate distance, the spectral area of the sextet (M0) corresponding to 8 nn Fe increases, while the spectral area of the sextet M3 representing Fe atoms with three and more Ag nearest neighbors decreases with increas-

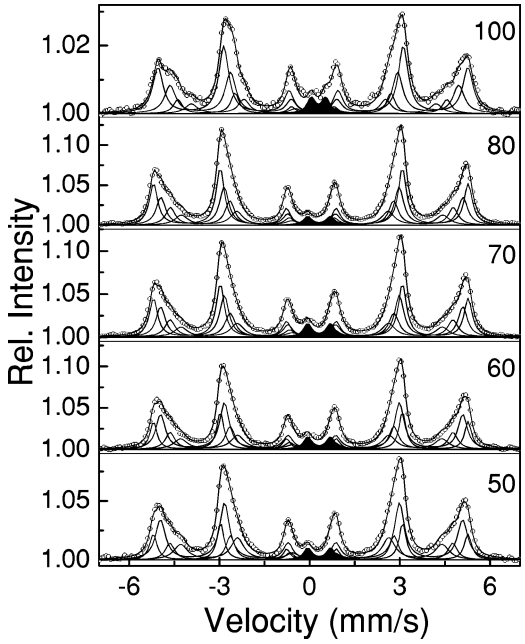

FIG. 7. Fitted CEMS of Fe/Ag multilayers of set C with $\Lambda = 5.0$ nm as a function of the target-substrate distance. The target-substrate distance is given in mm. The ^{57}Fe marker layer is placed in the middle of the specimen Fe layers. Experimental data points are shown by hollow spheres and fitted subspectra are indicated by solid lines.

ing distance. The spectral area of sextet M2 also decreases with distance, while that of the doublet remained constant within experimental error. The increment in the spectral area of sextet M0 suggests that intermixing decreases with distance. These changes in the CEMS may be understood considering the fact that the plasma particle density (flux) changes with the distance. The thickness of the deposited material per pulse also depends on the target-to-substrate distance. To deposit the same thickness with an increasing target-to-substrate distance means that the number of pulses for the individual elemental layer is higher and inversely proportional to the square of the target-to-substrate distance. During deposition the kinetic energy of the implanted material does not change much. Therefore, the implantation behavior of the ablated material or ions will remain unchanged while varying the target-to-substrate distance. Thus, the change at the interface may be affected mainly by the thermodynamic effects of the deposited solid. Due to the smaller thickness of the deposited material per pulse, there will be sufficient time to demix at the interface due to the positive heat of mixing of the solid solution, when the target-to-substrate distance increases. While depositing the materials onto the substrate one should not only consider the effects of the implantation on the substrate and the deposition of low-energy ions and materials but also the sputtering of the materials from the substrate, sometimes also called resputtering.[29] When the target-to-substrate distance is smaller, the number of atoms and ions on the substrate is higher. Therefore, the resputtering effects at the substrate will be more pronounced compared to the effects when the distance is larger. At a laser fluence of 4 J/cm^2, the number of ablated particles per square millimeter is two-times higher for Ag than for Fe and the difference increases with increasing laser fluence.[30] Therefore, while depositing the Ag layer on a substrate containing Fe at the top, the deposition reaction would include the diffusivity of Ag on Fe, which is

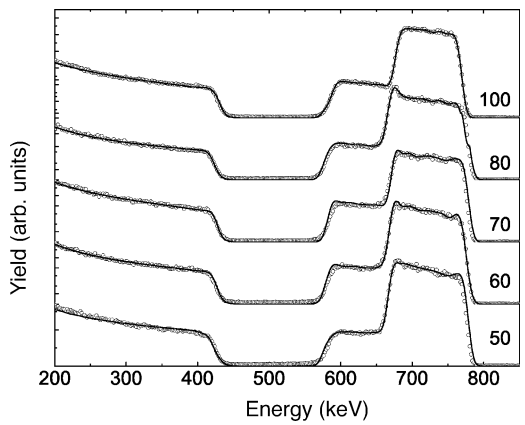

FIG. 8. The fitted RBS spectra of Fe/Ag multilayers with $\Lambda = 5.0$ nm as a function of the target-substrate distance (set C).

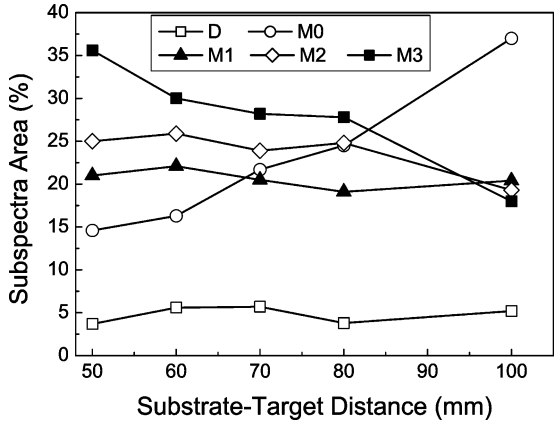

FIG. 9. The abundance of the different magnetic and nonmagnetic subspectra as a function of the target-substrate distance (set C). Details for M0, M1, M2, M3, and d are given in the text.

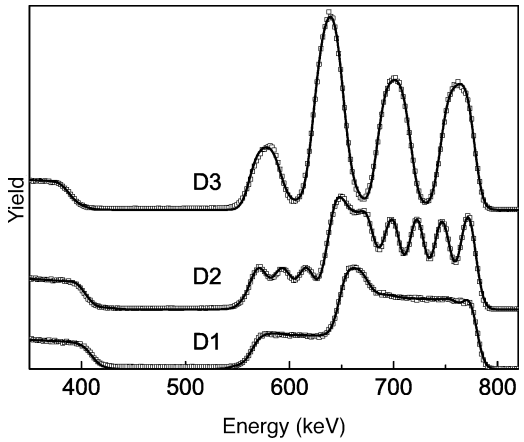

FIG. 10. The fitted RBS spectra of the Fe/Ag multilayers of set D.

TABLE III. Individual layer thicknesses evaluated from the RBS spectrum of specimen D3 (from surface to substrate). The values given in parentheses represent the standard deviation.

Element	Thickness (nm)
Ag	18(3)
Fe	21(3)
Ag	19(3)
Fe	22(3)
Ag	19(3)

lower than that of Fe on Ag, but the resputtering yield of Fe due to energetic Ag ions is considerably lower. Jordan *et al.*[31] and Lunney[32] have shown that sputtering may be important for the deposition rate in standard geometry. They demonstrated that self-sputtering by copper atoms from the plasma plume can reduce the copper deposition rate by a factor of 2. However, when resputtering plays a dominant role for the high-energy particles, the low-energy particle is important for the number of sticking particles on the substrate.

We have also deposited the multilayer specimens D1–D3 with a target-to-substrate distance of 68 mm. The sample geometry of specimens D1–D3 is exactly the same as that of specimen B3, where ^{57}Fe is placed in the center of the natural iron. The periodicity of samples D1–D3 is 9.4 nm ($N=10$), 19.5 nm ($N=5$), and 48.0 nm ($N=2$), respectively, as obtained by low angle x-ray-diffraction analysis, keeping the total thickness constant. RBS spectra of samples D1–D3 are shown in Fig. 10. From this figure one can easily observe the position of the individual layers of Fe and Ag in sample D3. The estimated thicknesses of the individual layers in sample D3, after fitting the RBS spectra, are given in Table III. Due to the energy straggling of the backscattered He^{++} ions, the depth resolution is too low to resolve the intermixed zone. Therefore, the thickness has been given assuming that there is no intermixing at the interface and assuming bulk densities of the elemental layers.

Figure 11 shows the CEMS of samples D1–D3, and their fit parameters are listed in Table II. It is seen that the spectra are quite sharp compared to the spectrum of specimen B3 and, therefore, while fitting the CEMS, we considered only two sextets (M0 and M1) along with doublet d. The relative

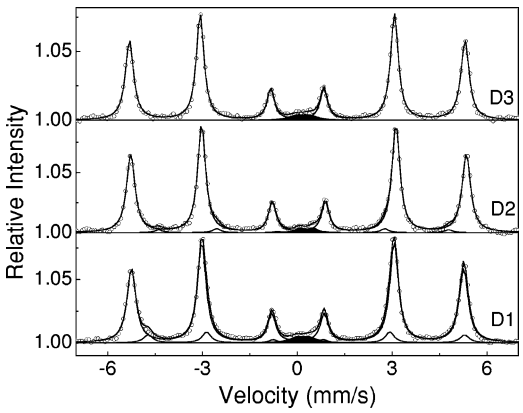

FIG. 11. The fitted CEMS of the Fe/Ag multilayers of set D.

area of M1 is smaller than that of M1 in sample B3. Thus, the concentration of Ag in Fe is considerably smaller in this case. The relative areas of M1 and d are similar in samples D2 and D3. The concentration of Ag in Fe is higher in set B than in set D. Thus, as the distance between target and substrate decreases, the diffusivity in the inverse direction increases compared to set B as observed in the case of set C also.

IV. CONCLUSION

We deposited Fe/Ag multilayers by pulsed laser deposition (PLD) by varying the geometry of the multilayers and by varying the target-to-substrate distance. Qualitatively, different diffusion rates for Fe in Ag and vice versa have been observed. The interface structure of the multilayers was affected by different implantation ranges and a different mobility of the elements in their counterparts. The target-to-substrate distance experiment proves that an increased distance leads to a sharper interface structure. So, to achieve the sharp interface structure one has to keep a lower instantaneous deposition rate.

ACKNOWLEDGMENTS

The authors are grateful to D. Purschke for expertly running the IONAS accelerator for the RBS measurements. This work was supported by the Sonderforschungsbereich 345 in Göttingen (Projects Nos. B8 and A11).

*On leave from Institute of Instrumentation, Devi Ahilya University, Indore 452017, India. Electronic address: gupta@physik2.uni-goettingen.de

†Electronic address: pschaaf@uni-goettingen.de URL: http://www.uni-goettingen.de/pschaaf

[1] P. Pronko, S. Dutta, D. Du, and R. K. Singh, J. Appl. Phys. **78**, 6233 (1995).

[2] R. Singh, O. Holland, and J. Narayan, J. Appl. Phys. **68**, 233 (1990).

[3] V. Y. Balandin, R. Niedrig, and O. Bostanjoglo, J. Appl. Phys. **77**, 135 (1995).

[4] T. Venkateshan, X. Wu, A. Inam, and J. Watchman, Appl. Phys. Lett. **52**, 1193 (1987).

[5] R. Neifeld, S. Gunapala, C. Liang, S. Shaheen, M. Craft, J. Proce, D. Simon, and W. T. Hill, III, Appl. Phys. Lett. **53**, 703 (1988).

[6] G. Xiao, J. Wang, and P. Xiang, Appl. Phys. Lett. **62**, 420 (1993).

[7] F. de Boer, R. Boom, W. Mattens, A. Miedema, and A. Niessen, *Cohesion in Metals* (North-Holland, Amsterdam, 1988).

[8] M. Neubauer, K.-P. Lieb, P. Schaaf, and M. Uhrmacher, Phys. Rev. B **53**, 10 237 (1996).

[9] K. Sumiyama, Vacuum **41**, 1211 (1990).

[10] S. Fähler and H.-U. Krebs, Appl. Surf. Sci. **96-98**, 61 (1996).

[11] H. Krebs, Y. Luo, M. Störmer, A. Crespo-Sosa, P. Schaaf, and W. Bolse, Appl. Phys. A: Mater. Sci. Process. **61**, 591 (1995).

[12] H.-U. Krebs, Int. J. Non-Equilib. Process. **10**, 3 (1997).

[13] M. Uhrmacher, K. Pampus, F. Bergmeister, D. Purschke, and K.

Lieb, Nucl. Instrum. Methods Phys. Res. B **9**, 234 (1995).
[14] N. P. Barradas, C. Jeynes, and R. P. Webb, Appl. Phys. Lett. **71**, 291 (1997).
[15] P. Schaaf, A. Krämer, L. Blaes, G. Wagner, F. Aubertin, and U. Gonser, Nucl. Instrum. Methods Phys. Res. B **53**, 184 (1991).
[16] F. Landry and P. Schaaf (unpublished).
[17] A. Crespo-Sosa, P. Schaaf, W. Bolse, K.-P. Lieb, M. Gimbel, U. Geyer, and C. Tosello, Phys. Rev. B **53**, 14 795 (1996).
[18] M. Neubauer, K.-P. Lieb, P. Schaaf, and M. Uhrmacher, Thin Solid Films **275**, 69 (1996).
[19] P. Schaaf, M. Weisheit, and H. U. Krebs, Acta Phys. Pol. A **100**, 751 (2001).
[20] P. Schurer, Z. Celinski, and B. Heinrich, Phys. Rev. B **48**, 2577 (1993).
[21] P. Schurer, Z. Celinski, and B. Heinrich, Phys. Rev. B **51**, 2506 (1995).
[22] S. Delage, B. Legrand, and F. Soisson, Phys. Rev. B **58**, 15 810 (1998).
[23] T. Detzel and N. Memmel, Phys. Rev. B **49**, 5599 (1994).
[24] G. Betz and K. Wien, Int. J. Mass Spectrom. Ion Processes **140**, 1 (1994).
[25] J. Ziegler, *The Stopping and Ranges of Ions in Matter* (Pergamon, NY, 1980).
[26] E. Ma, J.-H. He, and P. J. Schilling, Phys. Rev. B **55**, 5542 (1997).
[27] M. F. van Rapp, L. Socolovsky, F. Sanchez, and I. Toriani, J. Phys.: Condens. Matter **14**, 857 (2002).
[28] N. Wanderka, U. Czubayko, V. Naundorf, V. Ivchenko, A. Y. Yermakov, M. Uimin, and H. Wollenberger, Ultramicroscopy **89**, 189 (2001).
[29] K. Sturm and H.-U. Krebs, J. Appl. Phys. **90**, 1061 (2001).
[30] S. Fähler, K. Sturm, and H.-U. Krebs, Appl. Phys. Lett. **75**, 3766 (1999).
[31] R. Jordan, D. Cole, J. Lunney, K. Mackay, and D. Givord, Appl. Surf. Sci. **86**, 24 (1995).
[32] J. Lunney, Appl. Surf. Sci. **86**, 79 (1999).